

## Corrosion Inhibition Mechanism on Copper: Reactivity Trends of 1,3,4-Thiadiazole Inhibitors

Mustafa ELİK\* and Nihat KARAKUŞ<sup>2</sup>

<sup>1</sup>Department of Mathematics and Science Education, Faculty of Education, Sivas Cumhuriyet University, Sivas, Türkiye

<sup>2</sup>Department of Chemistry, Faculty of Science, Sivas Cumhuriyet University, 58140, Sivas, Turkey

\*(melik@cumhuriyet.edu.tr) Email of the corresponding author

(Received: 11 April 2025, Accepted: 23 April 2025)

(5th International Conference on Engineering, Natural and Social Sciences ICENSOS 2025, April 15-16, 2025)

**ATIF/REFERENCE:** Elik, M. & Karakuş, N. (2025). Corrosion Inhibition Mechanism on Copper: Reactivity Trends of 1,3,4-Thiadiazole Inhibitors. *International Journal of Advanced Natural Sciences and Engineering Researches*, 9(4), 141-151.

**Abstract-** This study combines DFT-based quantum chemical calculations with experimental data to analyze the inhibition behavior of thiadiazole derivatives on copper. Compound (2) exhibited the highest inhibition efficiency computationally and experimentally, showing strong agreement between theory and experiment. Parameters such as electrophilicity index, dipole moment, and Fukui functions correlate with surface adsorption and provide a mechanistic foundation for designing more efficient inhibitors.

**Keywords:** Corrosion Inhibition; Thiadiazole Derivatives; DFT; Proton Affinity, Fukui Functions.

### I. INTRODUCTION

The 1,3,4-thiadiazole ring system has emerged as a privileged heterocyclic scaffold in modern chemistry due to its versatile electronic configuration and chemical reactivity, mainly attributed to the presence of the  $-N=C-S$  functional group. Literature data indicate that these compounds exhibit various bioactivities, including antimicrobial, antifungal, antiviral, anti-inflammatory, analgesic, anticonvulsant, antioxidant, and diuretic effects [1-6]. Beyond pharmaceutical applications, 1,3,4-thiadiazole derivatives have also gained prominence in materials science, particularly as effective corrosion inhibitors [7-9]. Recent studies underscore their ability to form stable, adherent, and compact protective films on metal substrates, notably copper, under aggressive chloride-containing environments [10-12]. This is particularly interesting because copper, widely used in thermal, electrical, and mechanical systems, is highly susceptible to localized corrosion that compromises structural integrity and system longevity. Therefore, developing high-performance organic inhibitors tailored for copper is a subject of significant industrial and environmental relevance.

The corrosion inhibition efficiency of 1,3,4-thiadiazole derivatives is intricately governed by the interplay between their electronic structure and substituent-driven steric effects [13-17]. In particular, substituents at the 5-position modulate molecular orbital energies, frontier electron density distribution, and adsorption orientation, which critically impact the molecule-metal interaction strength. Alkyl substituents, with varied branching and inductive characteristics, alter the HOMO-LUMO gap, chemical hardness, and local reactivity indices, which ultimately determine the inhibitor's adsorption geometry and protective capability.

The main objective of this study is to investigate the corrosion inhibition efficiency of three 1,3,4-thiadiazole derivatives, considering their neutral, protonated, and copper-complexed forms on copper atoms using quantum chemical calculations. It is important to emphasize that, in the computational protocol, the copper atom is treated as a representative model for the brass surface, which is widely used in experimental setups. This approximation is scientifically justified since the copper (100) surface exhibits well-defined crystallographic properties that align well with DFT requirements, offering a stable and computationally tractable model for metal–inhibitor interactions. In this study, instead of using alloy surface models or hybrid quantum mechanics/molecular mechanics (QM/MM) approaches, copper-complexed species were explicitly constructed using a single Cu atom in coordination with the inhibitor molecules, as illustrated in the optimized geometries (Figure 1). These Cu complexes were fully optimized using the Gaussian software package, providing reliable structural and electronic data directly linked to their inhibition performance.

This work focuses on how electronic and structural properties such as proton affinity, frontier molecular orbitals, and charge distribution influence the interaction with the copper atom and determine inhibition performance. By comparing different molecular forms' reactivity and binding tendencies, this study aims to provide a theoretical foundation that aligns with experimental observations, ultimately supporting the rational design of effective copper corrosion inhibitors. In this context, 5-ethyl-1,3,4-thiadiazol-2-amine (1), 5-(ethylthio)-1,3,4-thiadiazol-2-amine (2), and 5-(tert-butyl)-1,3,4-thiadiazol-2-amine (3) were selected as representative model systems to systematically explore the structure–activity relationship using quantum chemical methods. Notably, the study examines the neutral forms and considers the protonated and copper-complexed species to comprehensively understand inhibition under different physicochemical states. Theoretical evaluations, particularly those involving frontier molecular orbitals, Fukui functions, and proton affinity calculations, offer valuable insight into how molecular reactivity translates into practical inhibition performance. The outcomes of this investigation reveal that these molecules have the potential to reduce corrosion rates significantly, with efficiencies reaching up to 90%, highlighting their superior performance and practical viability in real-world applications.

To ensure a reliable comparison with theoretical predictions, the experimental inhibition efficiencies (IE%) of the studied thiadiazole derivatives (1), (2), and (3) were derived by averaging data obtained from two complementary electrochemical methods: potentiodynamic polarization and electrochemical impedance spectroscopy. Based on the results reported by X. Joseph Raj and N. Rajendran, the average inhibition efficiencies were determined to be 65.5% for (1), 76.8% for (2), and 66.9% for (3) [17]. These values represent a consistent trend across both experimental techniques and provide a robust benchmark for evaluating the accuracy of quantum chemical descriptors in predicting corrosion inhibition performance on brass surfaces.

Ultimately, this study provides a mechanistic rationale for developing next-generation copper corrosion inhibitors based on the thiadiazole framework and bridges the gap between theoretical predictions and experimental observations through a detailed quantum chemical analysis. These quantum chemical calculations were conducted to establish a comprehensive reactivity profile for each molecular form: neutral, protonated, and copper-complexed. The derived descriptors, including band gap energy ( $\Delta E$ ), ionization potential (IP), chemical hardness ( $\eta$ ), electrophilicity ( $\omega$ ), and proton affinity (PA), were critically evaluated to rationalize the experimentally observed inhibition efficiencies. This approach enables a quantitative correlation between computed reactivity parameters and experimental IE% values, ultimately guiding the electronic interpretation of inhibitor–metal interactions.

## II. MATERIALS AND METHOD

All computations were performed using the Gaussian 16 software package [18], and molecular structures were visualized through GaussView 6.0.8 [19]. Solvent effects were modeled via the integral equation formalism polarized continuum model (IEF-PCM), allowing accurate simulation of aqueous-phase conditions relevant to corrosion environments [20]. Density Functional Theory (DFT) was employed due to its validated capability to accurately predict corrosion inhibitor activity through electron density analysis, which is widely used in corrosion studies. Geometry optimizations, Molecular Electrostatic Potential (MEP) analyses, and calculations of global reactivity descriptors band gap energy ( $\Delta E$ ), ionization potential (IP), electron affinity (EA), chemical hardness ( $\eta$ ), chemical softness ( $\sigma$ ), and electrophilicity indices ( $\omega^-$ ,  $\omega^+$ ) were carried out for the neutral, protonated, and copper-complexed forms of the studied 1,3,4-thiadiazole derivatives in their interactions with copper atom. These calculations were performed at the B3LYP/6-31G(d) computational levels in the gas phase and aqueous solution.

$$\Delta E_{gap} = E_{HOMO} - E_{LUMO} \quad (1) \quad \varepsilon = \frac{1}{\omega} \quad (8)$$

$$IP = -E_{HOMO} \quad (2) \quad \omega^- = \frac{(3IP + EA)^2}{(16(IP - EA))} \quad (9)$$

$$EA = -E_{LUMO} \quad (3) \quad \omega^+ = \frac{(IP + 3EA)^2}{(16(IP - EA))} \quad (10)$$

$$\eta = \left( \frac{IP - EA}{2} \right) \quad (4) \quad \Delta\omega^\pm = \omega^+ + \omega^- \quad (11)$$

$$\sigma = \frac{1}{\eta} \quad (5) \quad f^+ = q(N + 1) - q(N) \quad (12)$$

$$\mu = -\chi = \left( \frac{IP + EA}{2} \right) \quad (6) \quad f^- = q(N) - q(N - 1) \quad (13)$$

$$\omega = \frac{\mu^2}{2\eta} \quad (7) \quad f^0 = \frac{q(N + 1) - q(N - 1)}{2} \quad (14)$$

The global reactivity parameters were calculated using the equations (1–11) presented below. Additionally, Fukui functions ( $f^+$ ,  $f^-$ ,  $f^0$ ) were calculated using equations (12–14) to analyze local reactivity sites on the molecular structures.

Rooted in the Pearson hard and soft acid-base (HSAB) theory and governed by the principles of chemical potential equalization, the electron transfer interaction model offers a robust theoretical foundation for interpreting adsorption phenomena. For bulk copper, where the ionization potential (IP) equals the electron affinity (EA), the absolute electronegativity ( $\chi$ ) and global hardness ( $\eta$ ) are quantitatively defined as 4.43 eV and 0.0 eV, respectively. This equivalence simplifies the conceptual DFT treatment of copper–inhibitor interactions by enabling the direct application of reactivity indices to model charge transfer dynamics at the metal–molecule interface. [21–26].

$$\Delta N = \frac{\chi_{Cu} - \chi_{inh}}{2(\eta_{Cu} + \eta_{inh})} \quad (15)$$

Recent studies have replaced electronegativity ( $\chi$ ) with the work function  $\phi$  in evaluating adsorption efficiency, as the latter pertains more directly to the Fermi level of the metal. DFT calculations yield a work function value of 4.49 eV for the Cu (100) surface. The agreement between experimental data and  $\Delta N$  values calculated via the modified equation underscores the robustness of this computational strategy in predicting inhibitor performance, further validating the use of quantum descriptors in corrosion studies. [27-29].

$$\Delta N_{110} = \frac{\phi - \chi_{inh}}{2(\eta_{Cu_{100}} + \eta_{inh})} \quad (16)$$

The initial interaction energy ( $\Delta\psi$ ) was calculated using electronegativity and hardness parameters of the copper surface and the inhibitor molecules to quantify the molecule-metal interaction further. This equation captures the energetic driving force of charge transfer during adsorption. Given that the hardness ( $\eta$ ) of bulk copper is 0.0 eV, the resulting  $\Delta\psi$  values reflect the energetic favorability of the adsorption process, directly correlating with inhibition efficiency.

$$\Delta\psi = \frac{(\chi_{Cu} - \chi_{inh})^2}{4(\eta_{Cu} + \eta_{inh})} \quad (17)$$

This equation quantitatively defines the initial energetic interaction between the inhibitor molecule and the copper surface at the early adsorption stage. Considering that the global hardness ( $\eta_{Cu}$ ) of bulk copper is theoretically zero, the  $\Delta\psi$  parameter becomes entirely governed by the electrophilicity differential between the metal and the inhibitor. Consequently, this formulation captures the inherent thermodynamic favorability of electron transfer, reinforcing the mechanistic rationale for the superior adsorption affinity and inhibitory efficacy of the examined thiadiazole derivatives.

Proton affinity ( $PA$ ) values were calculated to precisely evaluate the protonation tendencies of the inhibitors, providing critical insights into their inhibition efficiencies, using equations (18–19):

$$PA = E_{pro} - (E_{non-pro} + E_{H^+}) \quad (18)$$

$$E_{H^+} = E_{H_3O^+} - E_{H_2O} \quad (19)$$

In this study, frontier molecular orbital analysis was performed utilizing Koopmans' Theorem, emphasizing that HOMO/LUMO energies and band gap energy ( $\Delta E$ ) significantly explain HOMO/LUMO interactions and the anti-corrosive properties of the investigated 1,3,4-thiadiazole derivatives.

### III. RESULTS AND DISCUSSION

The quantum chemical analysis provided valuable insight into the electronic and structural features of the three thiadiazole derivatives investigated: 5-ethyl- (1), 5-(ethylthio)- (2), and 5-(tert-butyl)-1,3,4-thiadiazol-2-amine (3). The optimized geometries and molecular electrostatic potential (MEP) surfaces of the neutral forms revealed that all derivatives possess nucleophilic regions localized primarily on the exocyclic amine nitrogen (N6), supporting their potential to engage in surface adsorption.

The copper-complexed geometries of compound (1), shown in Figure 1, illustrate distinct spatial arrangements depending on the molecular form (neutral, protonated, or complexed). HOMO–LUMO distributions confirm substantial orbital overlap with copper, particularly via sulfur and nitrogen coordination sites, which corroborates the proposed interaction mechanisms.

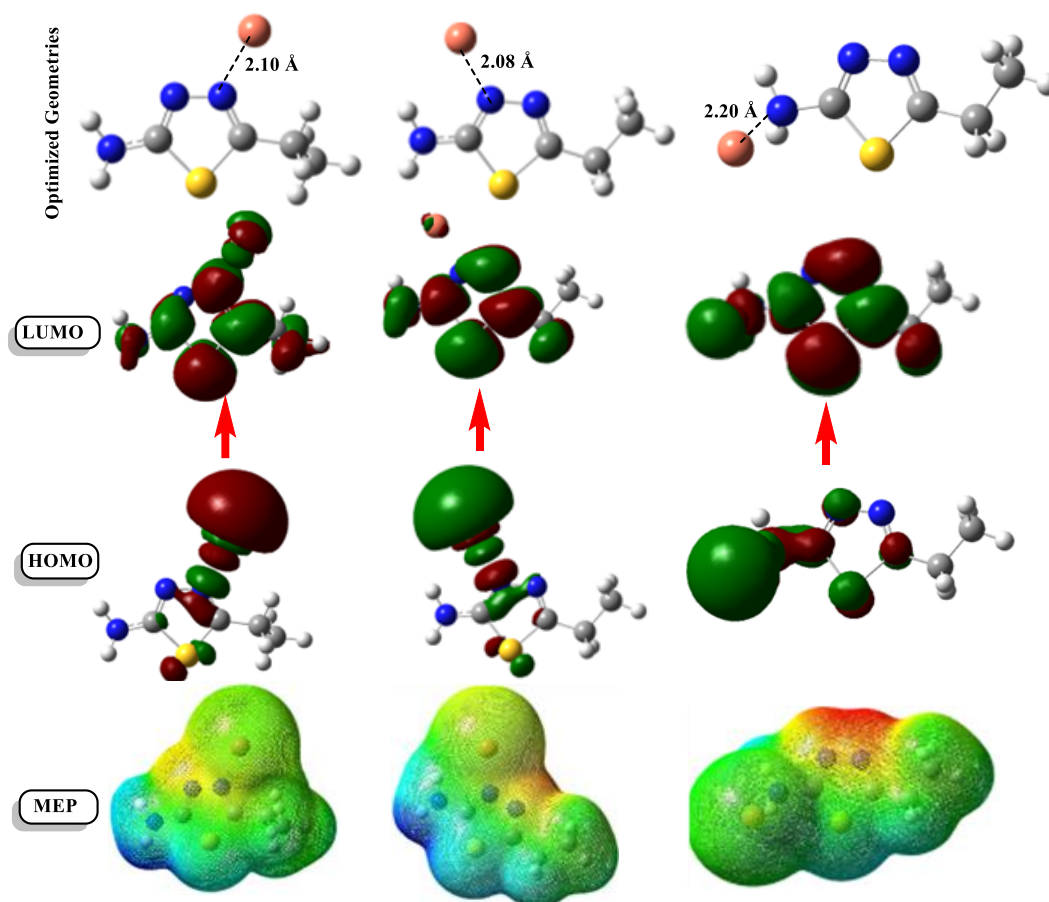


Figure 1. Optimized Geometries, Frontier Molecular Orbitals (HOMO–LUMO), and Molecular Electrostatic Potential (MEP) Maps of the Copper Complexes of Compound (1)

The Cu-complexed geometries of compounds (2) and (3), visualized in Figure 2, further validate these findings and suggest that steric bulk influences orbital delocalization and surface binding. Table 1 summarizes the global reactivity descriptors (GRDs) in gas and aqueous phases. Compound (2) exhibits the lowest HOMO–LUMO energy gap (5.34 eV in gas, 5.36 eV in aqueous), indicating greater reactivity. In contrast, compound (1) shows the highest dipole moment in water (4.39 D), which may enhance electrostatic adsorption. Compound (2) also has the highest electrophilicity index (1.99 eV), supporting its stronger tendency to accept electrons from copper atoms. These GRD trends align with experimental data. The condensed Fukui functions presented in Table 2 further pinpoint local reactive sites. For all compounds, the exocyclic amine nitrogen (N6) consistently shows high nucleophilic character ( $f^-$  values between  $-0.35$  and  $-0.44$ ), validating its role in metal coordination. Sulfur atoms (S3) also exhibit strong reactivity, especially in compounds (1) and (3), indicating dual-site adsorption pathways.

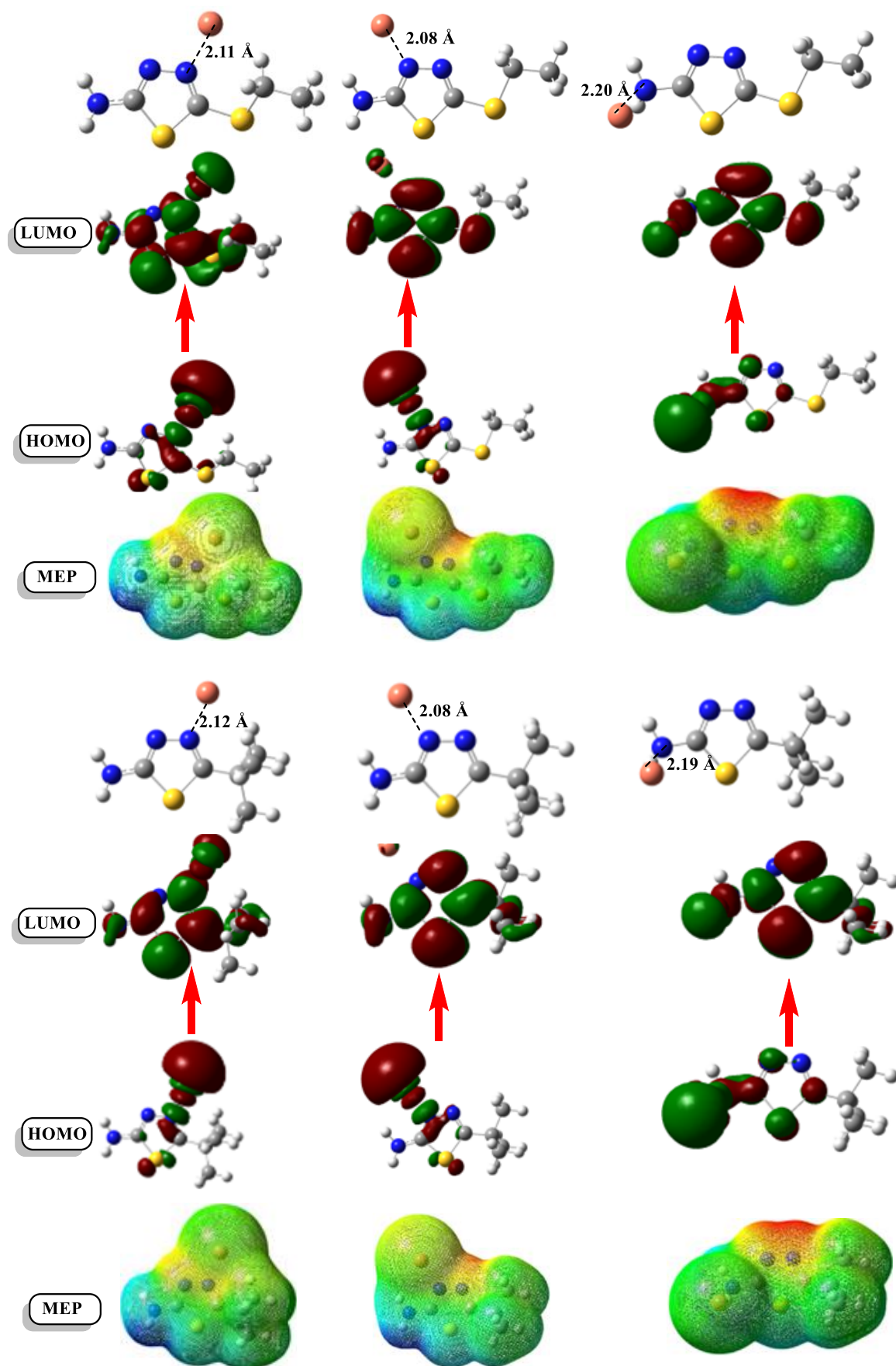


Figure 2. Optimized Geometries, Frontier Molecular Orbitals (HOMO–LUMO), and Molecular Electrostatic Potential (MEP) Maps of the Copper Complexes of Compound (2) and Compound (3).

Table 1. Comparison of Global Reactivity Descriptors for Compounds (1), (2), and (3) in Gas and Aqueous Phases at the B3LYP/6-31G(d) Level

GRDs*	B3LYP/6-31G(d) level					
	Gas Phase			Aqueous Phase		
	(1)	(2)	(3)	(1)	(2)	(3)
IP	6.250	5.823	6.224	6.289	5.946	6.293
EA	0.412	0.479	0.377	0.466	0.587	0.471
$\Delta E_{\text{gap}}$	5.838	5.344	5.846	5.824	5.359	5.822
$\eta$	2.919	2.672	2.923	2.912	2.679	2.911
$\sigma$	0.343	0.374	0.342	0.343	0.373	0.344
$\chi$	3.331	3.151	3.301	3.378	3.267	3.382
$\mu$	-3.331	-3.151	-3.301	-3.378	-3.267	-3.382
$\omega$	1.901	1.858	1.863	1.959	1.991	1.964
$\varepsilon$	0.526	0.538	0.537	0.511	0.502	0.509
$\omega^+$	0.600	0.617	0.579	0.634	0.693	0.637
$\omega^-$	3.931	3.768	3.879	4.012	3.959	4.019
$\Delta N$	1.604	1.709	1.651	1.532	1.559	1.526
$\Delta N_{110}$	1.691	1.789	1.738	1.619	1.639	1.613
$\Delta\psi$	0.103	0.153	0.109	0.095	0.126	0.094
$\mu$	<b>3.026</b>	<b>1.699</b>	<b>3.000</b>	<b>4.398</b>	<b>2.560</b>	<b>4.352</b>

\*All energy-based descriptors (IP, EA,  $\Delta E$ ,  $\eta$ ,  $\chi$ ,  $\mu$ ,  $\omega$ ,  $\omega^-$ ,  $\omega^+$ ,  $\Delta N$ , and  $\Delta N_{110}$ ) are given in electronvolts (eV); softness ( $\sigma$ ) and nucleophilicity index ( $\varepsilon$ ) are expressed in inverse electronvolts ( $\text{eV}^{-1}$ ); the initial interaction energy ( $\Delta\psi$ ) is reported in electronvolts (eV); dipole moment ( $\mu$ ) is presented in Debye.

Site-specific proton affinity (PA) values were calculated for each nitrogen center to investigate protonation behavior (Table 3). The results indicate that N6 is the most favorable site for protonation across all molecules, with the least negative PA values. The calculated initial interaction energy values ( $\Delta\psi$ ) support the energetic favorability of adsorption. Compound (2) showed a more negative  $\Delta\psi$  than the others, indicating a stronger thermodynamic driving force for surface interaction.

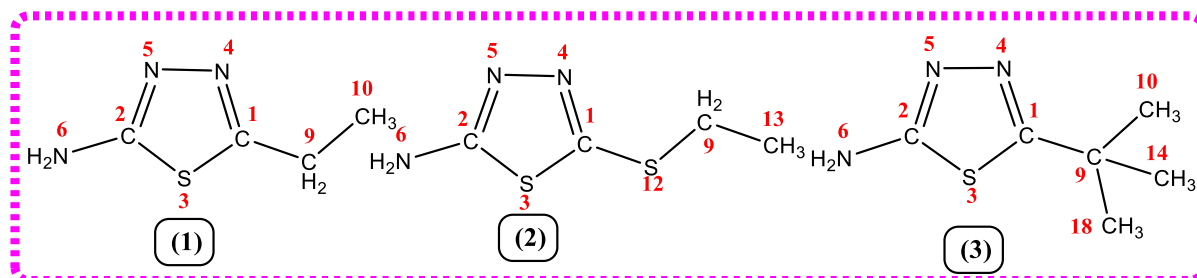


Figure 3. Atomic Site Numbering of the Investigated 5-Substituted 1,3,4-Thiadiazole Derivatives.

Table 2. Condensed Fukui Functions ( $f^+$ ,  $f^-$ ,  $f^0$ ) of Selected Atoms for Compounds (1)–(3) Based on NBO Charge Analysis

Inhibitor	Atom No	$f^+$	$f^-$	$f^0$
(1)	C1	-0,107	-0,189	-0,148
	C2	-0,174	0,033	-0,071
	S3	-0,739	0,333	-0,203
	N4	0,051	-0,249	-0,099
	N5	0,127	-0,364	-0,119
	N6	0,186	-0,443	-0,128
	C9	0,247	-0,185	0,031
	C10	0,247	-0,185	0,031
(2)	C1	-0,045	-0,079	-0,062
	C2	-0,158	0,02	-0,069
	S3	-0,665	0,295	-0,185
	N4	0,125	-0,328	-0,102
	N5	0,148	-0,325	-0,089
	N6	0,193	-0,355	-0,081
	C9	0,266	-0,253	0,007
	C13	-0,428	-0,036	-0,232
(3)	C1	-0,100	-0,229	-0,165
	C2	-0,174	0,035	-0,069
	S3	-0,735	0,349	-0,193
	N4	0,035	-0,231	-0,098
	N5	0,128	-0,353	-0,113
	N6	0,185	-0,434	-0,125
	C9	-0,043	0,084	0,021
	C10	0,373	-0,347	0,013
	C14	0,357	-0,351	0,003
C18	0,356	-0,350	0,003	

Table 3. Site-Specific Proton Affinity (PA) Values for Nitrogen Atoms in Compounds (1)–(3)

Inhibitor	Nitrogen atoms	PA (kJ/mol)
(1)	(N(1))	-246.81
	(N(2))	-248.36
	(N(3))	-128.87
(2)	-(N(1))	-242.96
	(N(2))	-246.69
	(N(3))	-132.76
(3)	-(N(1))	-256.52
	(N(2))	-255.85
	(N(3))	-133.09

This trend strongly correlates with the spatial electron density and nucleophilic character of the exocyclic amine (N(6)), which is not delocalized into the aromatic ring system and thus retains higher lone-pair availability. MEP surface analysis further validates this site-selectivity, revealing a dominant negative potential localized at N(6), indicative of its proton-capturing capacity. These findings agree with established basicity principles and reinforce the structure–function paradigm wherein protonation at N(6) enhances interaction affinity with electrophilic centers on the copper surface, particularly under low pH conditions.

In conclusion, the exocyclic amine (N(6)) is unequivocally the preferred protonation site across all derivatives, and this site-specific behavior plays a pivotal role in modulating the inhibitor's adsorption strength, surface charge transfer, and overall inhibition efficiency. Therefore, targeting this basic center in future inhibitor design strategies represents a rational and mechanistically grounded approach for enhancing anticorrosive performance in acidic environments.

A clear correlation emerges when comparing these theoretical findings to experimental inhibition efficiencies reported by Raj and Rajendran (2011). Compound (2) demonstrated the highest experimental IE% (76.8%), followed by (3) (66.9%) and (1) (65.5%). This trend is consistent with the theoretical descriptors: (2) had the highest electrophilicity and nucleophilicity at key atoms, the smallest energy gap, and the strongest Cu binding tendency. These results validate the computational strategy used and highlight the relevance of DFT-based descriptors in accurately predicting inhibitor performance.

In summary, the theoretical results not only reproduce the experimental inhibition trends but also offer mechanistic insight into the role of electronic structure in determining anticorrosive activity. Compounds with better orbital overlap, stronger electron-accepting character, and high basicity at key nitrogen sites demonstrated superior performance, reinforcing the structure–activity relationship essential for designing next-generation corrosion inhibitors.

#### IV. CONCLUSION

The electronic structure and reactivity of the three studied 1,3,4-thiadiazole derivatives demonstrate that alkyl substituents significantly impact their corrosion inhibition potential. The results suggest that electron-donating alkyl groups enhance adsorption through HOMO interaction with copper atoms. Fukui analysis supports these findings by indicating enhanced nucleophilic sites correlating with improved inhibition efficiency. These insights provide a basis for designing next-generation copper corrosion inhibitors derived from thiadiazole scaffolds.

#### ACKNOWLEDGEMENT

We are grateful to TUBITAK ULAKBIM, High Performance and Grid Computing Center (TR-Grid e-Infrastructure), for providing the computational resources necessary for our calculations. Their support has been invaluable to the success of our work.

#### REFERENCES

- [1] Desai, N. C., Jadeja, D. J., & Shah, K. N. (2024). Synthesis and Biological Evaluation. *S-Heterocycles: Synthesis and Biological Evaluation*, 17.
- [2] Moulay, S. (2015). Covalent Functionalizations of Poly (vinyl chloride) in Tune with Applications: An Update. *Journal of Research Updates in Polymer Science*, 4(2), 79.
- [3] Hipler, F., Winter, M., & Fischer, R. A. (2003). N–H···S hydrogen bonding in 2-mercapto-5-methyl-1, 3, 4-thiadiazole. Synthesis and crystal structures of mercapto functionalised 1, 3, 4-thiadiazoles. *Journal of molecular structure*, 658(3), 179-191.
- [4] Ibrahim, A. G., Elgammal, W. E., Hashem, A. H., Mohamed, A. E., Awad, M. A., & Hassan, S. M. (2024). Development of a chitosan derivative bearing the thiadiazole moiety and evaluation of its antifungal and larvicidal efficacy. *Polymer Bulletin*, 81(2), 1303-1325.
- [5] Chandurwala, S., Balachandran, H., Gowramma, B., Yokkesh, M., Pranav, V., Vinethmartin, J., & Kaviarasan, L. (2025). A Recent Progress in Biological Activities of 1, 3, 4-thiadiazole and its Derivatives: A Review. *Current Topics in Medicinal Chemistry*.
- [6] Shia, J. S., Ibrahim, M. S., & Al-Darraj, A. S. (2023). Various of Chemical and Pharmacological Applications of 1, 3, 4-Thiadiazole and It's Derivative. *South Asian Res J Pharm Sci*, 5(6), 240-248.
- [7] Hu, Y., Li, C. Y., Wang, X. M., Yang, Y. H., & Zhu, H. L. (2014). 1, 3, 4-Thiadiazole: synthesis, reactions, and applications in medicinal, agricultural, and materials chemistry. *Chemical reviews*, 114(10), 5572-5610.

- [8] Hu, Y., Li, C. Y., Wang, X. M., Yang, Y. H., & Zhu, H. L. (2014). 1, 3, 4-Thiadiazole: synthesis, reactions, and applications in medicinal, agricultural, and materials chemistry. *Chemical reviews*, 114(10), 5572-5610.
- [9] Tang, H., Sun, J., Yan, X., & Wu, P. (2019). Electrochemical and adsorption behaviors of thiadiazole derivatives on the aluminum surface. *RSC advances*, 9(59), 34617-34626.
- [10] Talebian, M., Raeissi, K., Atapour, M., Fernández-Pérez, B. M., Betancor-Abreu, A., Llorente, I., ... & Souto, R. M. (2019). Pitting corrosion inhibition of 304 stainless steel in NaCl solution by three newly synthesized carboxylic Schiff bases. *Corrosion Science*, 160, 108130.
- [11] Assad, H., Thakur, A., Bharmal, A., Sharma, S., Ganjoo, R., & Kaya, S. (2022). Corrosion inhibitors: fundamental concepts and selection metrics. *Corrosion Mitigation; De Gruyter*, 19-50.
- [12] 2. Palomar-Pardavé, M., et al. (2012). Influence of the alkyl chain length of 2-amino-5-alkyl-1,3,4-thiadiazole compounds on the corrosion inhibition of steel immersed in sulfuric acid solutions. *Corrosion Science*, 54, 231-243.
- [13] Bentiss, F., Mernari, B., Traisnel, M., Vezin, H., & Lagrenée, M. (2011). On the relationship between corrosion inhibiting effect and molecular structure of 2, 5-bis (n-pyridyl)-1, 3, 4-thiadiazole derivatives in acidic media: Ac impedance and DFT studies. *Corrosion Science*, 53(1), 487-495.
- [14] Qadr, H. M., & Mamand, D. M. (2023). A computational study of substituent effect 1, 3, 4-thiadiazole on corrosion inhibition. *Azerbaijan Chemical Journal*, (2), 19-29.
- [15] Nyijime, T. A., Chahul, H. F., Ayuba, A., & Iorhuna, F. (2023). Theoretical investigations on thiadiazole derivatives as corrosion inhibitors on mild steel. *Advanced Journal of Chemistry-Section A*, 6(2), 141-154.
- [16] Salman, T. A., Zinad, D. S., Jaber, S. H., Al-Ghezi, M., Mahal, A., Takriff, M. S., & Al-Amiery, A. A. (2019). Effect of 1, 3, 4-thiadiazole scaffold on the corrosion inhibition of mild steel in acidic medium: An experimental and computational study. *Journal of Bio-and Tribo-Corrosion*, 5(2), 48.
- [17] Raj, X. J., & Rajendran, N. (2011). Corrosion inhibition effect of substituted thiadiazoles on brass. *International Journal of Electrochemical Science*, 6(2), 348-366.
- [18] Frisch MJ, Trucks GW, Schlegel HB, Scuseria GE, Robb MA, Cheeseman JR, Scalmani G, Barone V, Petersson GA, Nakatsuji H, Li X, Caricato M, Marenich AV, Bloino J, Janesko BG, Gomperts R, Mennucci B, Hratchian HP, Ortiz JV, Izmaylov AF, Sonnenberg JL, Williams Ding F, Lipparini F, Egidi F, Goings J, Peng B, Petrone A, Henderson T, Ranasinghe D, Zakrzewski VG, Gao J, Rega N, Zheng G, Liang W, Hada M, Ehara M, Toyota K, Fukuda R, Hasegawa J, Ishida M, Nakajima T, Honda Y, Kitao O, Nakai H, Vreven T, Throssell K, Montgomery Jr, JA, Peralta JE, Ogliaro F, Bearpark MJ, Heyd JJ, Brothers EN, Kudin KN, Staroverov VN, Keith TA, Kobayashi R, Normand J, Raghavachari K, Rendell AP, Burant JC, Iyengar SS, Tomasi J, Cossi M, Millam JM, Klene M, Adamo C, Cammi R, Ochterski JW, Martin RL, Morokuma K, Farkas O, Foresman JB, Fox DJ (2016) *Gaussian 16 Rev. C.01*, Wallingford, CT
- [19] Dennington R, Keith T, Millam J (2016) *GaussView 6.0*. 16, Semichem. Inc., Shawnee Mission KS
- [20] Tomasi J, Mennucci B, Cammi R (2005) Quantum mechanical continuum solvation models. *Chem Rev* 105(8):2999-3094.
- [21] Pearson, R. G. (1963). Hard and soft acids and bases. *Journal of the American Chemical society*, 85(22), 3533-3539.
- [22] Pearson, R. G. (1985). Absolute electronegativity and absolute hardness of Lewis acids and bases. *Journal of the American Chemical Society*, 107(24), 6801-6806.
- [23] Pearson, R. G. (1989). Absolute electronegativity and hardness: applications to organic chemistry. *The Journal of Organic Chemistry*, 54(6), 1423-1430.
- [24] Pearson, R. G. (1997). *Chemical hardness* (Vol. 10, No. 3527606173). Weinheim: Wiley-VCH.
- [25] Hadisaputra, S., Purwoko, A. A., Savalas, L. R. T., Prasetyo, N., Yuanita, E., & Hamdiani, S. (2020). Quantum chemical and Monte Carlo simulation studies on inhibition performance of caffeine and its derivatives against corrosion of copper. *Coatings*, 10(11), 1086.
- [26] Tan, B., Zhang, S., Cao, X., Fu, A., Guo, L., Marzouki, R., & Li, W. (2022). Insight into the anti-corrosion performance of two food flavors as eco-friendly and ultra-high performance inhibitors for copper in sulfuric acid medium. *Journal of colloid and interface science*, 609, 838-851.
- [27] Tao, X. M., Tan, M. Q., Zhao, X. X., Chen, W. B., Chen, X., & Shang, X. F. (2006). A density-functional study on the atomic geometry and adsorption of the Cu (1 0 0) c (2 × 2)N Surface. *Surface science*, 600(17), 3419-3426.

- [28] Da Silva, J. L., Schroeder, K., & Blügel, S. (2004). First-principles investigation of the multilayer relaxation of stepped Cu surfaces. *Physical Review B Condensed Matter and Materials Physics*, 69(24), 245411.
- [29] Duan, X., Warschkow, O., Soon, A., Delley, B., & Stampfl, C. (2010). Density functional study of oxygen on Cu (100) and Cu (110) surfaces. *Physical Review B—Condensed Matter and Materials Physics*, 81(7), 075430.